Catalysis Letters Vol. 112, Nos. 1–2, November 2006 (© 2006)
DOI: 10.1007/s10562-006-0156-1

Catalytic deNO$_x$ properties of novel vanadium oxide based open-framework materials

M. Ishaque Khan,[a,*] Saadia Tabussum,[a] Christopher L. Marshall,[b] and Michael K. Neylon[b]

[a]*Department of Biological, Chemical and Physical Sciences, Illinois Institute of Technology, Chicago, IL 60616, USA*
[b]*Chemical Engineering Division, Argonne National Laboratory, Argonne, IL 60439, USA*

Received 17 May 2006; accepted 20 September 2006

The deNO$_x$ catalytic properties of a new class of open-framework structure materials, $Li_6[Mn_3(H_2O)_{12}V_{18}O_{42}(XO_4)] \cdot 24H_2O$ (X = V, S) (**1**), $[Fe_3(H_2O)_{12}V_{18}O_{42}(XO_4)] \cdot 24H_2O$ (X = V, S) (**2**), $[Co_3(H_2O)_{12}V_{18}O_{42}(XO_4)] \cdot 24H_2O$ (X = V, S) (**3**), and $Li_6[Ni^{II}_3(H_2O)_{12}V^{VI}_{16}V^{V}_2O_{42}(SO_4)] \cdot 24H_2O$ (**4**), have been studied. The crystal structures of these novel systems consist of three-dimensional arrays of vanadium oxide clusters $\{V_{18}O_{42}(XO_4)\}$, as building block units, interlinked by {–O–M–O–} (M = Mn, **1**; M = Fe, **2**; M = Co, **3**; M = Ni, **4**) bridges. Their open-framework structures contain cavities, similar to those observed in conventional zeolites, which are occupied by exchangeable cations and/or readily removable water of hydration. The catalysts derived from these materials were tested for the selective catalytic reduction (SCR) of nitrogen oxides $\{NO_x\}$ into N_2 using a hydrocarbon, propylene, as the reducing agent. The catalysts were ineffective under lean burn conditions. However, the new catalysts, especially the one derived from the cobalt derivative (**3**), showed intriguing deNO$_x$ activity under rich conditions. They remove up to ~ 99% of the toxic NO$_x$ emissions in 1.5% O_2 with 100% selectivity to N_2. The active phase of the catalysts exhibit good stability, can be readily regenerated, and are selective to the desired product-N_2. The catalytic reactions occur at moderately low temperatures (400–500 °C). The catalysts were characterized by FT-IR, temperature programmed reactions (TPR and TPO), SEM, BET surface area measurements, elemental analysis, and X-ray diffraction (XRD). Additional advanced techniques were used to further characterize the catalyst phases that showed most promising deNO$_x$ activity and increased tolerance to oxygen.

KEY WORDS: vanadium oxides; framework materials; deNO$_x$; selective catalytic reduction; NO$_x$.

1. Introduction

Increased environmental concerns and stricter government regulations require industry and society to develop high efficiency zero/minimal-waste industrial processes. Consequently, there is a wide-spread need for a new generation of efficient catalysts to meet the environmental and technological challenges ranging from the removal of toxic gases from auto exhaust and industrial flue gas streams to selective oxidation of hydrocarbons and removal of urea from blood [1–5]. These goals could possibly be achieved by the design and synthesis of new catalyst grade materials with well-defined structures whose properties can be readily modified at the atomic and molecular level.

The deNO$_x$ process- the removal of toxic NO$_x$ (mainly NO and NO_2) gases from the flue gas streams of fossil fuel plants, chemical processing factories, and exhaust of automobile engines is an area of intense current interest [2]. Although the direct decomposition of these species into the elemental constituents is both attractive and thermodynamically favored (reaction 1) [6], the reaction is kinetically very slow [7], even in the presence of a variety of catalysts [8].

$$NO \longrightarrow 1/2N_2 + 1/2O_2 \quad \Delta H = -21.6 \text{ Kcal/mol} \quad (1)$$

In stationery industrial applications such as fossil-fuel power plants, the widely employed selective catalytic reduction (SCR) of NO$_x$ is carried out on a catalyst surface (mostly transition metal oxides supported on porous anatase [5] type titanium dioxide support; e.g., $V_2O_5/WO_3/TiO_2$ deNO$_x$ catalyst [9]) by a reductant-most commonly ammonia, introduced to the flue gases (reaction 2) [2,10].

$$6NO_x + 4NH_3 \xrightarrow{\text{Catalyst}} 5N_2 + 6H_2O \quad (2)$$

Although it removes 65–80% of NO$_x$ gases from the flue gas streams, the discharge ("slip") of unreacted ammonia into the environment is a major drawbacks of the SCR process [10a,10d]. Ammonia is comparable to NO$_x$ in its toxicity ($TLV_{NH_3} = 20$ mg/m^3 and $TLV_{NO_x} = 5$ mg/m^3; TLV = Threshold Limit Value). The problem of the toxic emission in SCR process is exacerbated when enhanced NO$_x$ removal (90–95%) is desired (as required by the new environmental regulations), as it will be at the expense of ammonia slip and possible carbon monoxide (CO) discharge.

Selective catalytic reduction by hydrocarbons (HC-SCR) is an evolving alternative to ammonia based SCR process [6] for the removal of NO$_x$ gases. It is

*To whom correspondence should be addressed.
E-mail: khan@iit.edu

1011-372X/06/1100–0001/0

viewed as a more environmentally friendly process [2,5–8] which uses readily available and environmentally acceptable hydrocarbons (such as propylene, instead of ammonia) as the reducing agent. The HC-SCR can also be easily used in diesel systems to reduce NO_x emissions. The major disadvantage here is the lack of suitable catalysts [8]. The catalysts that have been tested in recent years suffer either from the deactivation by O_2, SO_2, H_2O, inactivity at the desired temperatures or produce undesirable byproducts (CO, N_2O, NO_2). The effectiveness of the catalysts is also diminished by water (hydrothermal deactivation) because of reversible retardation caused by competitive adsorption between water and NO or hydrocarbon. Water also causes irreversible deactivation due to dealumination of zeolite catalysts and aggregation of metal ions in the zeolite framework.

Therefore, the search for suitable catalyst materials for application in HC-SCR deNO$_x$ continues. A cleaner and efficient NO_x disposal requires the development of new catalysts that can selectively catalyze the reduction of NO_x in an environmentally benign and cost-effective manner. A catalyst that will make defixation/reduction of NO_x commercially viable and environmentally acceptable will have enormous impact on the environment and the society.

Since vanadium is the active site in the most commonly employed NH_3-SCR-deNO$_x$ catalyst or plays an important role in the conversion of NO_x [5a,7a], vanadium oxide based materials are considered potentially attractive deNO$_x$ catalysts [2,5–8]. These same catalysts have not been examined for activity using hydrocarbons as the reductant. They may have advantage over the transition metal exchanged zeolites (e.g. Cu-ZSM-5) that have been studied in recent years with limited success. One of the major drawbacks of the zeolite catalyst materials is that their suitability is determined empirically with practically little or no possibility of improvements in their performance by introducing structural changes at the molecular level [10]. The mechanism of interactions of these catalysts with substrate molecules and the structures of the catalytic sites are poorly understood, due mainly to the complex nature of these empirical catalysts that are inaccessible to many physico-chemical techniques.

On the other hand, the design and synthesis of well defined catalyst grade materials suitable for industrial scale applications remain a challenge to the synthetic chemists. This difficult problem has attracted considerable attention in recent years. Recently, a series of a new class of vanadium oxide based crystalline open-framework materials have been synthesized by molecular building block or "bottom-up" approach [11]. These new materials, which are composed of well-defined building block units, have been characterized by elemental analysis, FT-IR spectroscopy, thermogravimetric analysis, manganometric titration, temperature dependent magnetic susceptibility measurement, X-ray powder diffraction, bond valence sum calculations, and complete single crystal XRD structure analysis. Their structures are resolved to the extent of atomic resolution by a combination of spectroscopic and physico-chemical methods and complete single crystal structure analyses.

The crystals of the new materials have open-framework structures containing well-ordered three-dimensional arrays of the building block clusters $\{V_{18}O_{42}(XO_4)\}$ ($X = VO_4^{3-}$, SO_4^{2-}, Cl^-, Br^-, or H_2O) which are interlinked by {–O–M–O–} (M = Mn, Fe, Co, Ni, Zn, etc.) bridging groups or linkers. Each cluster in these structures is connected to six others to generate the three-dimensional open-framework which contain cavities and channels, similar to those observed in conventional zeolites (aluminosilicates). The channels are occupied by exchangeable counter ions and/or readily removable lattice water molecules. The cavities and channels in these solids can be varied by changing the building blocks at the molecular level.

They three-dimensional frameworks in these materials contain reactive metal sites – incorporated in the building block units – which are exposed to the interior of the voids present in their structures. The type and nature of these metal sites (e.g. Mn, Fe, Co, Ni, Zn, etc.,) can be readily varied by choosing the appropriate building units and linkers. In essence, these materials provide a unique opportunity of integrating atomistic design of active sites and fine-tuning their redox potentials. They also allow us to tailor the size of the cavities and channels in these solids. This unprecedented level of control over framework architecture coupled with systematic variation of chemical composition and accurate characterization techniques give us unique opportunity to develop a fundamental understanding of the structure–property relationships at the molecular level. These materials thus represent a new class of advanced materials which may be viewed as combining the reactivity of transition metals with the salient features of zeolites.

Given the established role of vanadium oxides in catalysis and catalyst supports [2,5–8] the new materials are attractive with potential use as deNO$_x$ catalysts for the HC-SCR process. Since they contain monodispersed controllable reactive sites, these systems provide excellent models of pristine materials suitable for studies on fundamentals of catalysis required for tailor-making catalytic surfaces with desirable and controllable properties and functions. Therefore, we have started a systematic study focused on evaluating the potential application of the new series of materials in the catalytic deNO$_x$ process. Instead of using toxic ammonia, which is used as reductant in the currently employed industrial scale SCR process, we have used an environmentally benign hydrocarbon, propylene, as reductant in our HC-SCR deNO$_x$ studies.

Here, we report the results of HC-SCR deNO$_x$ catalysis work done on the following representative

examples of the novel series of vanadium oxide based open-framework materials (OFM):

$$Li_6[Mn_3^{II}(H_2O)_{12}V_{16}^{VI}V_2^{V}O_{42}(XO_4)]\cdot 24H_2O(X{=}VO_4{,}SO_4) \quad (\mathbf{1})$$

$$[Fe_3(H_2O)_{12}V_{9.5}^{VI}V_{8.5}^{V}O_{42}(XO_4)]\cdot 24H_2O(X = VO_4, SO_4) \quad (\mathbf{2})$$

$$[Co_3(H_2O)_{12}V_{9.5}^{VI}V_{8.5}^{V}O_{42}(XO_4)]\cdot 24H_2O(X = VO_4, SO_4) \quad (\mathbf{3})$$

$$Li_6[Ni_3^{II}(H_2O)_{12}V_{16}^{VI}V_2^{V}O_{42}(SO_4)]\cdot 24H_2O \quad (\mathbf{4})$$

The deNO$_x$ catalytic activities of the new catalysts have been evaluated under different HC-SCR conditions. The catalytic properties of the new systems have also been compared to Cu-ZSM-5 and activated carbon. The catalysts were characterized by FT-IR, TGA, temperature programmed reactions (TPR and TPO), SEM, BET surface area measurements, elemental analysis, and X-ray diffraction. The catalyst phases showing the most promising deNO$_x$ activity and increased tolerance to oxygen were further characterized by advanced techniques.

The preliminary results presented here are part of an ongoing work. We expect that our continuing investigation will shed more lights to answer some intriguing observations and questions that arise from this work. The ongoing studies will enable us to better understand the potential and properties of the new materials and the catalysts derived from these systems.

2. Experimental section

2.1. Catalyst preparation

The following novel series of vanadium oxide based OFM **1–4**, were prepared by the methods we have described elsewhere [11].

$Li_6[Mn_3(H_2O)_{12}V_{18}O_{42}(XO_4)]\cdot 24H_2O(X{=}V,S)$ (**1**)[11a]

$[Fe_3(H_2O)_{12}V_{18}O_{42}(XO_4)]\cdot 24H_2O(X = V, S)$ (**2**) [11b]

$[Co_3(H_2O)_{12}V_{18}O_{42}(XO_4)]\cdot 24H_2O(X = V, S)$ (**3**) [11b]

$[Li_6[Ni_3(H_2O)_{12}V_{18}O_{42}(SO_4)]\cdot 24H_2O$ (**4**) [11c]

Following procedure, used to prepare the cobalt derivative (**3**) – which yielded the catalyst with the highest deNO$_x$ activity – illustrates the general synthetic method used for their preparation [11b,12].

An aqueous solution (3 mL) of LiOH · H$_2$O (5 mmol) was added slowly with stirring to a slurry of V_2O_5 (2.5 mmol) in 10 mL of water maintained between 84 and 86 °C. After the resulting light yellow solution was treated with hydrazine sulfate (2.5 mmol), the reaction mixture was further heated under continuous stirring for 10 min and diluted with deionized water to 25 mL (pH 4.6). The dark colored mixture was subsequently treated with $CoSO_4\cdot 6H_2O$ (1.25 mmol) and heated for 3–7 h. The reaction vessel containing the dark solution was stoppered and allowed to stay at room temperature for 12 h to yield crystals of 3. The crystals were isolated from the mother liquor and dried in air at the room temperature.

The solid state crystal structure of **3** consists of an open-framework containing three-dimensional arrays of the constituent clusters $\{V_{18}O_{42}(XO_4)\}$ ($X = VO_4^{3-}$, SO_4^{2-}) interlinked by {–O–Co–O–} bridging groups. The $\{V_{18}O_{42}\}$ cage of the cluster is made of 18$\{VO_5\}$ square pyramids sharing edges. The vanadium atoms of the cage exhibit mixed valence (V and IV oxidation states). The cobalt atoms, interlinking the constituent clusters, are present in the +2 oxidation state and in the octahedral geometry.

The OFMs which led to the most promising deNO$_x$ activity were identified and further characterized. Commercially available V_2O_5 [Cerac, −200 mesh], V_2O_3 [Cerac, −200 mesh] and activated charcoal [BIO-RAD], and 127% exchanged Cu-ZSM5 catalyst were also tested for the deNO$_x$ activities under similar conditions. The ammonium form of ZSM-5 with a Si/Al = 25 was provided by Zeolyst International. To obtain the H-form, the zeolite was calcined at 550 °C for 4 h in a static furnace. Cu was ion-exchanged into the zeolite according to commonly used literature procedures. To obtain a 60% exchanged Cu-ZSM-5 sample (following the commonly used nomenclature where 100% exchanged stands for one Cu ion per every two Al sites), hereafter referred as Cu(60)-ZSM-5, 100mL of a 0.015 M $Cu(NO_3)_2\cdot 2.5H_2O$ (99.99%, Aldrich) solution were stirred vigorously with 10 g of H-ZSM-5 (Si/Al = 25) for 2 h before adjusting dropwise the pH to 8 using a 0.8 M NH_4OH (30%, AR, Mallinkrodt) solution while stirring. The slurry was kept under stirring for an additional 24 h period. The solid was filtered, rinsed with water and dried at 100 °C. Samples were calcined for 4 h at 450–500°C. The number of exchange steps performed and/or the concentration of the metal solution was modified in order to achieve different metal loadings. The deNO$_x$ activities were compared with the activities of OFM **1–4**.

2.2. Sample treatment

The deNO$_x$ activity tests were carried out on as prepared samples of **1–4** and on the catalyst samples reduced in C_3H_6 at 400 °C. Catalysts samples were also reduced in H_2 at 400 °C in order to deduce the effect of the type of reductant gas on catalytic performance.

2.3. Catalyst characterization

The materials that exhibited the best deNO$_x$ activity and increased tolerance for oxygen were characterized

using BET surface area, FT-IR, elemental analysis, temperature programmed reduction (TPR) and oxidation (TPR & TPO), SEM, and XRD. Five point BET surface areas were performed on catalyst materials **1**–**4** using nitrogen physisorption method on a Micromeritics ASAP 2010 instrument. Infrared spectra (KBr pellets; 400–4000 cm^{-1} region) were recorded on a Nexus® 470 Spectrometer. The IR spectra were analyzed using the Thermonicolet OMNIC software. Elemental analysis on all the compounds was performed using a Perkin Elmer 2400 elemental analyzer and a Perkin Elmer optima 3300DC DCP Spectrometer. The TPR and TPO reactions were carried out on Altamira AMI-1 unit equipped with a TCD detector from Analytical Instruments. The outlet gas analysis was done by an attached inline GCMS (Stanford Research OMS200 Residual Gas Analyzer).

SEM images were obtained using a JEOL JSM-5900LV Scanning Electron Microscope. The XRD patterns of the best performing catalyst were recorded on a Siemens D5000 powder XRD at room temperature between 5 and 80° 2θ at 3 s count for every 0.02°.

2.4. Catalyst testing

DeNO$_x$ activities were measured at a space velocity of 10,000 h^{-1} at a flow rate of 100 cc/min. The deNO$_x$ activity tests were carried out under both lean and rich conditions using both as prepared and reduced catalyst samples. Unless otherwise specified, 1000 ppm of each NO$_x$ and C_3H_6 were used for all the deNO$_x$ activity tests. The composition of the flue gas stream comprised of He, NO/He, C_3H_6/He, O_2/He for lean condition and He, NO/He, C_3H_6/He for rich condition having the set gas flow rates and concentrations shown in table 1. Data on the product gases was collected on a micro GC equipped with a TCD detector from Analytical Instruments and the nitrogen oxides (NO and NO_2) were measured with a NOVA 300 CLD Chemiluminescent NO and NO$_x$ analyzer.

3. Results and discussion

3.1. Catalytic DeNO$_x$ activity tests-lean conditions

OFMs **1**–**4** were initially tested for deNO$_x$ activity under lean conditions (2% O_2) and rich conditions (O_2 free). The best performing catalyst materials (highest deNO$_x$ activity under all desirable conditions and selectivities towards N_2 and CO_2) were further characterized. All catalysts were tested using several oxygen and propylene concentrations to optimize the catalytic reaction conditions and determine the effect of the feed concentration on catalyst performance. The highest deNO$_x$ activities were observed after the catalyst materials were pre-reduced using propylene. In order to determine the effect of reductant, the use of H_2 was also examined.

Table 1 lists the conditions utilized for deNO$_x$ activity measurements for OFMs **1**–**4** under lean deNO$_x$ conditions. Under all temperatures examined (200–600 °C) all materials exhibited either no or marginal deNO$_x$ activity. The catalysts showed high selectivity to CO and CO_2. Nitrogen selectivity was to the less desirable NO_2 product.

Table 1
Gas compositions for deNO$_x$ activity tests under lean and rich conditions

Gas	Concentration of gases (%)	Lean condition set flow rate (cc/min)	Rich condition set flow rate (cc/min)
He		54.3	94.7
O_2/He	5.02	39.4	0.0
NO/He	5.02	2	2.0
C_3H_6/He	3.33	3.3	3.3

3.2. Catalytic DeNO$_x$ activity tests-rich conditions

Since the catalysts performed poorly under lean conditions, a study was conducted to determine catalyst activity under rich conditions using the gas composition and flow rates described in table 1. The deNO$_x$ activities of **1**–**4** were then compared with the NO$_x$ conversion rates of activated charcoal and Cu-ZSM-5 under similar experimental conditions.

Figure 1 shows the deNO$_x$ activity of **1**–**4** under rich conditions. The highest deNO$_x$ activity was obtained from **3** (the cobalt derivative of the OFM composed of $\{V_{18}O_{42}X\}$ clusters linked by –O–Co–O– groups). **3** showed a maximum deNO$_x$ activity at 500 °C with 100% selectivity to N_2.

The deNO$_x$ activities of **1**, **2**, and **4** are significantly lower than **3** and their activities increase with increasing temperature. **1**, **2** and **4** showed maximum activities at the highest tested temperature (600 °C). **1** had the least deNO$_x$ activity of 22.9% at 600 °C with 21.3% selectivity towards N_2. **2** and **4** had a maximum deNO$_x$

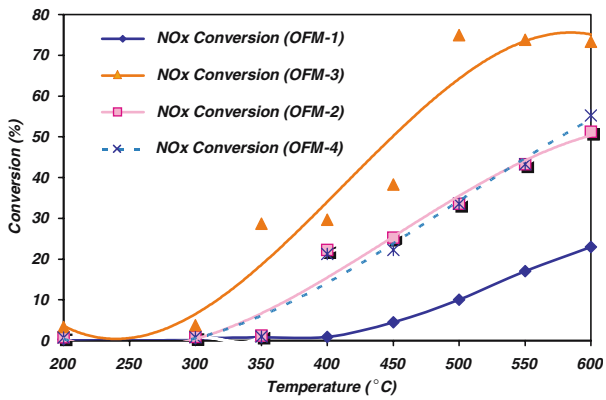

Figure 1. NO conversions over temperature for catalyst materials **1**–**4** under rich conditions.

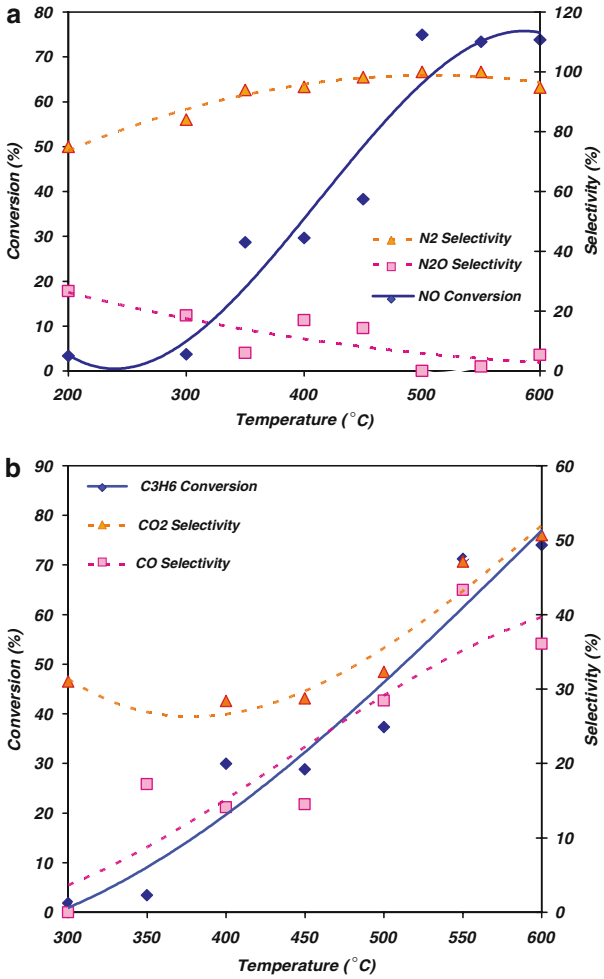

Figure 2. (a) NO conversion and its selectivity to N_2 and NO_2 over temperature for catalyst material **3** under rich conditions. (b) C_3H_6 conversion and its selectivity to CO and CO_2 over temperature for catalyst material **3** under rich conditions.

activity of 33.6% at 600 °C with selectivities of 31.5% and 31.2%, respectively, towards N_2.

Figure 2(a, b) show NO_x and propylene conversions and selectivities for **3** under rich conditions. The deNO$_x$ activity of **3** was less than 3.5% at temperatures below 300 °C (figure 2(a)). The activity slowly increases reaching a maximum of 74.9% at 500 °C and then drops as the temperature is further increased. Between 475 and 500 °C, NO_x conversion is 100% selective to N_2. At other temperatures small amounts of N_2O (less than 10%) are also observed.

As shown in figure 2(b), maximum propylene conversion (74.0%) was achieved at 600 °C with 37.0% and 26.7% selectivity towards CO_2 and CO, respectively. At maximum deNO$_x$ activity (500 °C), the propylene conversion was only 37.3% with selectivities to CO_2 and CO of 12.6% and 10.6% respectively. As before, this material undergoes significant coking. The maximum amount of coking was observed at 400 °C with 58% selectivity to coke.

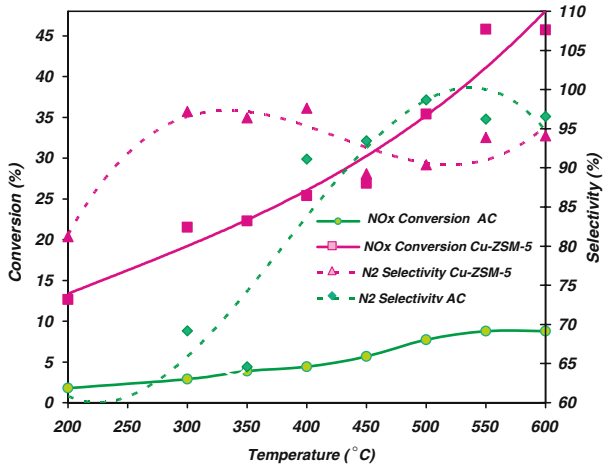

Figure 3. NO conversion and its selectivity to N_2 over temperature for catalyst materials Activated Charcoal (AC) and Cu-ZSM-5 under rich conditions.

Figure 3 is shows NO_x conversion and selectivity of N_2 for activated charcoal and Cu-ZSM-5 under rich conditions. The activated charcoal shows a maximum deNO$_x$ activity of 8.5% at 600 °C with selectivities of 100% for N_2 and CO. The amount of CO and CO_2 obtained from C_3H_6 conversion in case of activated charcoal was much different than the other materials. The high yields of CO and CO_2 indicate that the activated charcoal was limiting coke formation. Cu-ZSM-5 gave a maximum NO_x conversion of 45.7% with 93.9% selectivity to N_2 at 550 °C. However, under rich conditions, the deNO$_x$ activity by Cu-ZSM-5 decreased rapidly to 10.0% within 30 min. The high level of coking on the sample is the most probable reason for the decrease in the catalyst activity [7a,8].

Longevity tests at highest deNO$_x$ activity conditions (i.e. 500 °C) showed a gradual decrease in activity for all of the catalyst samples (**1**–**4**). This decrease in the deNO$_x$ activity of the catalyst materials **1**–**4** over time under rich condition may be attributed to the possible oxidation of the vanadium oxide based materials. Therefore, we pre-reduced the catalyst materials (**1**–**4**) with C_3H_6 for an hour. The reduced materials were then tested under rich conditions specified in table 1. Pre-reduced **2**, **3**, **4** showed a very high deNO$_x$ activity (>99%) with 100% selectivity to N_2 and a very high selectivity towards CO_2 at 500 °C.

Figure 4(a) shows NO_x conversions and N_2 selectivities for pre-reduced **1** and **3**. Initially, the increase in temperature leads to increased NO_x conversion up to 500 °C. The selectivity to N_2 runs almost parallel to conversion which is 100%, between 475 and 500 °C. Above 500 °C there is a drop in deNO$_x$ activity while N_2 selectivity remains 100%. The conversion and selectivity trend with materials **2** and **4** was similar to that of **3**. The NO_x conversion and selectivity pattern of **1** is much different than **2**–**4**. It showed lowest deNO$_x$ activity of ~25.0% with 12.5% selectivity for N_2 at 600 °C.

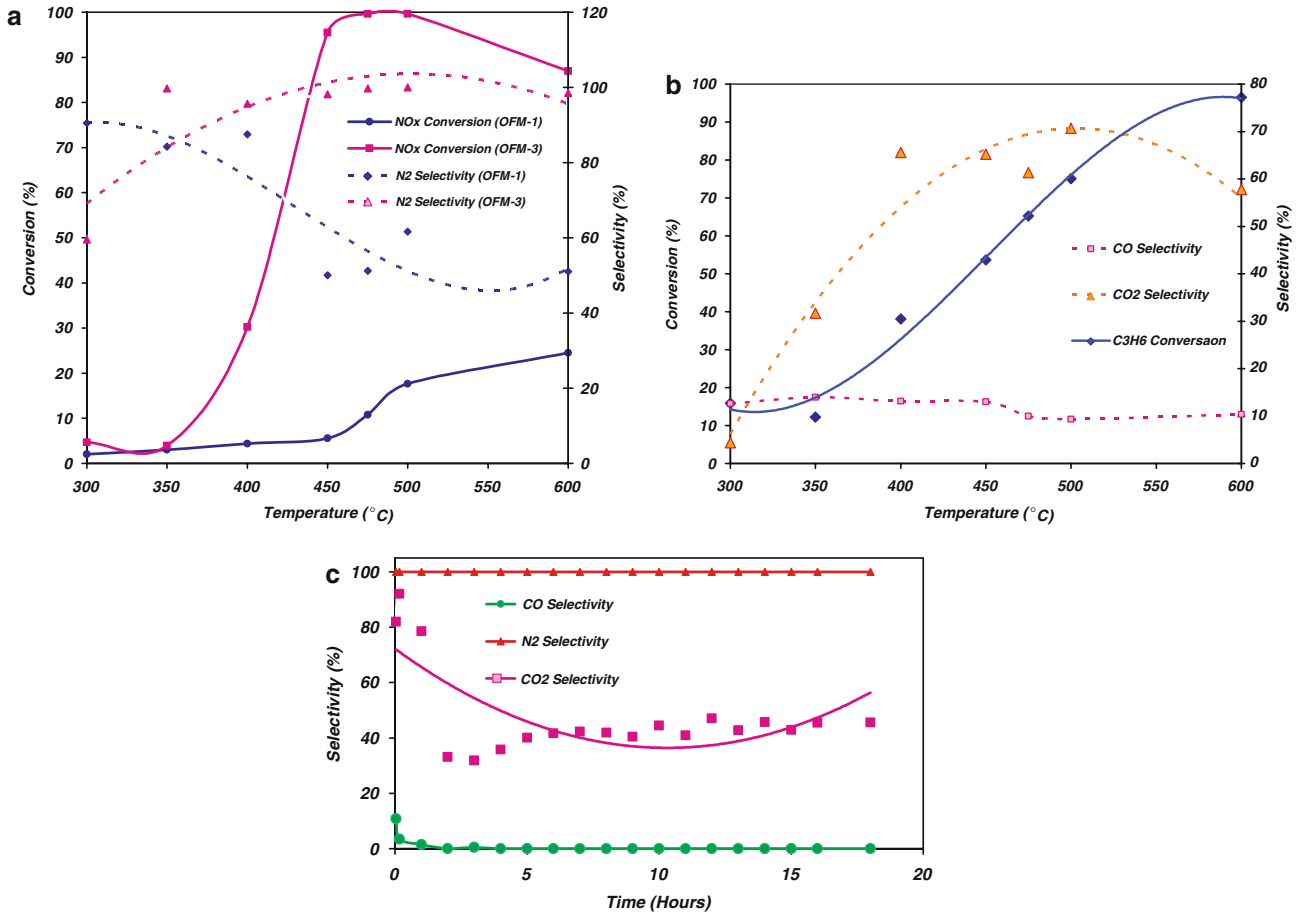

Figure 4. (a) NO conversion and its selectivity to N_2 over temperature for C_3H_6 reduced catalyst material **1** and **3** under rich conditions. (b) C_3H_6 conversion and its selectivity to CO and CO_2 over temperature for C_3H_6 reduced catalyst material 3 under rich conditions. (c) Selectivities for C_3H_6 reduced catalyst material **3** under rich conditions over time.

Figure 4(b) shows the C_3H_6 conversion and its selectivity to CO and CO_2. At 600 °C C_3H_6 conversion was around 96.5% with 55.8% and 10.0% selectivity for CO_2 and CO respectively. At 500 °C, when the deNO$_x$ activity is at its peak, the C_3H_6 conversion is 75% with a selectivity of 53.0% and 7.0% towards CO_2 and CO, respectively.

C_3H_6 supplied was not accounted for by the total carbonaceous products obtained. The hydrocarbon recovery was less than 100% as the C_3H_6 conversion was not consistent with its selectivity to CO or CO_2. The absence of any other carbonaceous byproduct indicated the retention of unaccounted hydrocarbon on the catalyst, either in the form of coke, hydrocarbon, or some other polymeric carbon form. This was confirmed by elemental analysis.

The C_3H_6 conversion is highly selective towards CO_2 rather than CO, the opposite to the trend observed under the lean conditions. As indicated in figure 4(b), an increase in temperature increases the selectivity for CO_2, from ~1% at 300 °C to 53% at 500 °C.

Further testing of catalysts **2**–**4** to see theirperformance over longer periods of time established **3** as themost stable catalyst for activity maintainance over an extendedperiod of time. Figure 4c shows how the deNO$_x$ activity of**3** is accompanied by the consistent selectivity to N_2 andCO_2. All of the NO$_x$ converted (>99%) is selectivelyconverted (100%) to N_2. The formation of N_2 by reductionof NO$_x$ remained at 100% level throughout the 18 h testperiod. Catalyst sample **3** was tested further beyond 18 h(after 1- 4-, and 6 weeks). In this duration the reactortube with the sample of **3** was covered with Para film and leftin air at room temperature). These longevity tests showed thatcatalyst **3** maintains its high deNO$_x$ activity, withoutneed for any further reduction, for a prolonged time (beyond 6 weeks).

Once reduced, catalyst 3 is not affected by exposure to atmospheric oxygen during sample handling. However, prolonged exposure to air does decreases its deNO$_x$ activity to some extent (<5%). The deNO$_x$ activity is restored to the 99% NO$_x$ conversion level by heating the partially deactivated catalyst in the presence of C_3H_6 at 400 °C for 5–10 min. The conversion of C_3H_6 at 500 °C starts at a high (75.0%) level and reduces to 36% after 18 h with high selectivity to CO_2. Initially, there were low selectivities to CO (~7%). The CO formation dropped after 20 min on stream, reaching

the 0% level within 90 min and maintained this level throughout the experiment. About 53.0% CO_2 formed in the beginning of the experiment increased to 85.0% within the first half hour. The CO_2 selectivity then slowly decreased to ~33% within 2 h and remained relatively constant throughout the test period.

The NO_x conversion was not affected and selectivity to N_2 remained the same (i.e. 100%) as long as the temperature and propylene concentration were maintained. Since the maximum propylene conversion for the **2**–**4** was around 75% even during maximum conversion at 500 °C, deNO$_x$ activity tests examined at varying concentrations of propylene to determine the optimum propylene concentration needed to maintain high deNO$_x$ activity. The total flow rate of 100 cc/min was maintained throughout the experiment by adjusting the flow rate of He diluent. The results of the experiments performed on OFM **3** under rich condition are shown in figure 5 in the form of a plot of percentage NO_x conversion versus C_3H_6 concentration. It shows the effect of propylene concentration on NO_x conversion.

The highest NO_x conversion was observed at a propylene concentration level of 600 ppm. Although somewhat lower concentrations of propylene also give excellent NO_x conversions (e.g. 99.2% at 450 ppm C_3H_6 and 98.8% at 300 ppm C_3H_6) for a short time, the level of deNO$_x$ activity dropped to 72.5% within 2 h and continue to drop rapidly thereafter. Thus the optimum concentration of propylene needed for achieving a sustainable high level of deNO$_x$ activity is 600 ppm. The rapid decrease in NO_x conversion can be attributed to several factors. It is possible that the lower C_3H_6 concentration leads to oxidation of the active metal sites of the catalyst. These sites are not brought back into the catalytic cycle owing to the presence of insufficient amount of propylene needed for rapid reduction of the oxidized metal centers. Furthermore, the propylene would also be needed for the continuous deposition of carbonaceous material which appears to be a dynamic process. Finally, as indicated by the plot in figure 5, **3** is not a NO_x decomposition catalyst since propylene is required for NO_x conversion. If C_3H_6 is not supplied the deNO$_x$ activity (or NO_x conversion) drops rapidly to zero.

To determine the oxygen tolerance of the catalysts, we introduced oxygen in varying concentrations (2–0.5%) into the reaction system while maintaining a constant total flow rate of 100 cc/min through the reactor. The data in figure 6 show that catalyst **3**, which was pre-reduced in C_3H_6, was more tolerant to the presence of excess oxygen. It maintained its high NO_x conversion level in the presence of up to 1% of oxygen. In the presence of 1.5% oxygen (lean condition) the deNO$_x$ activity of the C_3H_6 reduced catalyst **3** starts slowly dropping after 1.5 h. The catalyst was regenerated (i.e. re-reduced) when the NO_x conversion dropped below the desired level (80%).

To explore the effect of reductant type on catalyst activity, deNO$_x$ activity tests were also performed under rich conditions (as specified in table 1) on catalysts **1** and **3** after their pre-reduction in H_2 at 400°C for 3 h. Initially, **3** showed a low deNO$_x$ activity (28.5%). After an induction period of 45 min the deNO$_x$ activity reached a maximum of >99% and remained at this level throughout the test period indicating that both reduced metal and propylene are necessary for maintaining high deNO$_x$ activity. As long as the temperature is maintained at 500 °C and the experimental conditions are unchanged, the NO_x conversion is not affected and its selectivity towards N_2 remains same (~100%).

Under rich conditions, material**1** behaves differently from the other catalyst materials (**2**–**4**). Initially the deNO$_x$ activity of **1** (pre-reduced in H_2) is very low (~3%). Over a period of 1 h the NO_x conversion increased to 32.1% with selectivities of 25.0% for N_2 and 6.6% for N_2O. A maximum 51.1% NO_x conversion with selectivities of 47.5% for N_2 and 12.3% for N_2O was seen after 1.3 h. The NO conversion drops to 45.1% within 1.4 h and remains at this level for 3.2 h. The NO

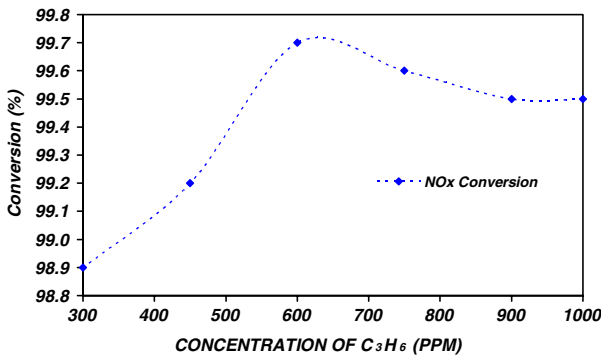

Figure 5. Percentage NO_x conversion for C_3H_6 reduced catalyst material **3** under rich conditions at 500 °C over different concentrations of propylene.

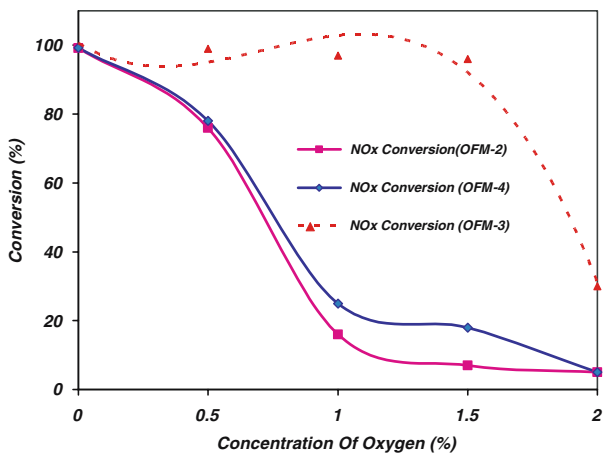

Figure 6. NO conversions over different oxygen concentrations for C_3H_6 reduced catalyst material **2**, **3** and **4** under rich conditions.

conversion decreases to 16% within 4 h with selectivity of 10.5% for N_2O and 5.9% for N_2.

Thus **1** and **3** show different deNO$_x$ activity pattern when pre-reduced with H_2 instead of C_3H_6 . The deNO$_x$ activity of **3** remains at 99% after an initial 45 min induction period indicating that C_3H_6 is needed for the high NO conversion rates. For the **1** a maximum of 51% NO$_x$ conversion is reached in 1.25 h dropping to 16% within 4 h.

The catalyst material **3** has the presence of the heterometal cobalt in –V–O–Co–O–V– environment. In order to establish whether just the presence of cobalt as heterometal in vanadium oxide framework would bring about the high deNO$_x$ activity or cobalt needs to be present in specific chemical environment. We tested different cobalt containing vanadium oxide based materials for deNO$_x$ catalytic activity. The results revealed that only the materials containing –V–O–Co–O-V– moieties showed high deNO$_x$ activity.

Table 2 lists the turnover frequency (TOF) per gram of metal for the four new catalysts along with the Cu-ZSM-5 catalyst. Catalyst material **3** is still the most active per gram of vanadium of the four new materials. It is an order of magnitude less active than the Cu in Cu-ZSM-5. The low activity can be partly explained by the increased surface area of the zeolite based system (45 m^2/g for **3** versus 398 m^2/g for Cu-ZSM-5). The low activity might also be due to the relatively low activity of vanadium for reduction of NO$_x$. Under lean conditions, Cu-ZSM-5 shows very high activity [13] where these V materials are inactive. Vanadium catalysts are better known for their oxidation activity and less for their ability to promote reduction of molecules such as NO$_x$. It is only when the V is in the presence of the Co in sample 3 that reasonable deNO$_x$ activities are observed. This activity may have more to do with the Co than the V phase of the catalyst. Future work will further investigate the effect of the Co phase of the catalyst.

3.3. Characterization of active catalysts phases

3.3.1. Surface area measurements

Surface areas were measured for **1**–**4** for as prepared, after reduction and after catalysis (table 3). As prepared materials have low surface areas possibly due to the presence of water of crystallization and coordinated water in their channels. The removal of water during the degassing step could lead to modifications in the framework structure. The surface areas increased significantly after the samples were reduced in C_3H_6 (in case of **3** there was a 10-fold increase in the surface area) showing an overall increase in the porosity of the active catalyst phase.

Table 2
Activity comparisons

	400 °C		500 °C	
	Conversion (%)	TOF g NO/g V metal Hr	Conversion (%)	TOF g NO/g V metal Hr
OFM-1	1	271	10	2706
OFM-2	22	6012	30	8198
OFM-3	30	8227	75	20,568
OFM-4	22	6276	30	8559
AC	4	n/a	7	n/a
Cu-ZSM-5	22	80787	35	12,8524

Table 3
Surface areas of materials OFM **1**–**4**

Sample	5-point BET surface area (m^2/g)			
	As prepared	C_3H_6 reduced	H_2 reduced	After catalysis
OFM-**1**	4	4	4	–
OFM-**2**	4	29	4	–
OFM-**3**	4	45	4	44
OFM-**4**	4	23	–	39

3.3.2. FT-IR analysis

The FT-IR spectrum of the as prepared sample, C_3H_6 reduced and after catalysis samples of **3** is shown in figure 7. The spectrum of the active catalyst after reduction in C_3H_6 is shown as figure 7(b). The spectrum of freshly prepared **3** (figure 7(a)) gives bands centered at 3419 and 1604 cm^{-1} due to absorbed water. A strong peak at 974 cm^{-1} was attributed to terminal υ(V=O) . Weak bands at 839 and 705 cm^{-1} and a broad band centered at 591 cm^{-1} are due to the bridging vanadium oxygen groups.

The spectrum of active catalyst phase obtained after the C_3H_6 reduction of **3** shows noticeable changes in the

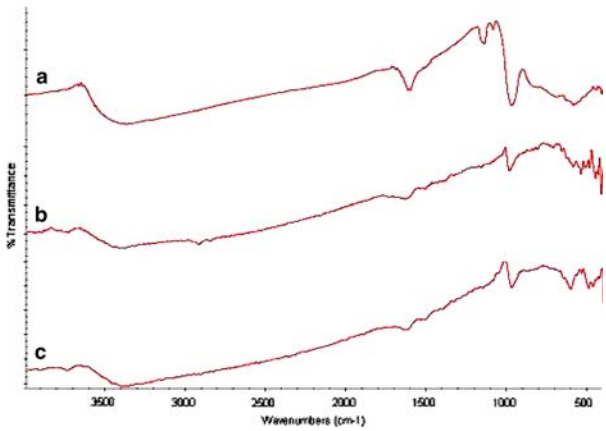

Figure 7. Infrared spectra (a) As synthesized catalyst material **3**; (b) Catalyst material **3** reduced in C_3H_6 indicating structural changes during reduction; (c) Catalyst material **3** after NO$_x$ reduction indicating significant changes in 600–400 cm^{-1} region.

1000–450 cm^{-1} region. Besides the appearance of additional bands, the feature due to the terminal υ(V=O) groups is absent indicating the loss of terminal (V=O) groups of the $\{V_{18}O_{42}X\}$ clusters during reduction. Also the bands due to lattice water are missing, as expected. The spectrum of C_3H_6 reduced **3** (figure 2(c)) also shows the absence of bands due to the terminal υ(V=O) groups and lattice water.

3.3.3. Elemental analysis

The elemental analysis for C, H and N was done on a sample of C_3H_6 reduced **3**. The elemental results indicated absence of H and N but were high in carbon content. The absence of N and H indicates that the carbon present is not a hydrocarbon or a cyanide phase. Different crystals of C_3H_6 reduced **3** of the same batch gave different percentage of carbon content indicating that the carbon deposition is not homogeneous.

3.3.4. Temperature programmed reduction

The TPR of **3** was initially carried out in H_2 in a temperature range of 30–600 °C. The results indicated a small reduction at 234 °C and an additional reduction peak starting at ~583 °C. Little information could be obtained from mass spectra data of the off-gases. The TPR was repeated in C_3H_6 and C_3H_8 to see the effect of different reductant gases on the catalyst **3**. The behavior of C_3H_6 reduced catalyst was completely different from the H_2 reduced catalyst. The TCD signal shows reduction over a range of temperature starting from 458 to 658 °C.

From the mass spectra data of the off-gases for the TPR of **3** in C_3H_6 (figure 8(a)) it is noted that CO_2 formation begins at 332 °C. The rate of CO_2 formation decreases at intermediate temperatures increasing again above 680 °C. C_3H_6 also undergoes cracking yielding CH_4 as cracking by-product. A large amount of H_2 is formed starting at 411 °C. The H_2 formation decreased a little at 674 °C but increases again at 730 °C. CO formation could not be established by mass spectra (since CO and N_2 have the same m/e and the C_3H_6 gas had N_2 balance).

The TPR of **3** in propane is much different from the TPR data of propylene (figure 8(b)). A very high amount of H_2 is formed starting at 484 °C. The TCD signal indicates that catalyst reduces between 129 and 135 °C and 400 and 500 °C. There is CO_2 formation starting at 486 °C, C_2H_2 formation at 847 °C, and H_2O formation at 532 °C. Thus there was a vast change in reduction pattern of **3** when different reductants were used.

3.3.5. Temperature programmed oxidation (TPO)

TPO of **3** was done initially on a H_2 reduced sample in temperature range of 30–600 °C. The TCD signal showed oxidation beginning at 187 °C which completed by 472 °C. Once again (like in case of TPR by H_2), any useful mass spectral data could be obtained from the mass spectra of exit gases.

As the reduction process and the materials formed after the reduction by H_2 and C_3H_6 are different, the catalyst sample **3**, reduced in C_3H_6 was taken and a TPO reaction was carried out (figure 8(c)). The TCD signal indicated oxidation at 303–435 °C, 488 and 649 °C. The oxygen consumption peaks correspond to this. The interesting information that could be obtained from mass spectra data is that there is a CO_2 loss starting at 285 °C and then again at 385 °C.

The XRD patterns of **3** as prepared, after reduction in C_3H_6 and after deNO$_x$ catalysis are shown in figure 9. The XRD pattern of as prepared **3** (Figure 9a) shows it to be a porous crystalline material. While the XRD patterns of the C_3H_6 reduced catalyst **3** (figure 9(b)) and the C_3H_6 reduced catalyst **3** after catalysis (figure 9(c)) indicates significant reduction in crystallinity of **3**.

3.3.6. Scanning electron microscopy (SEM)

SEM pictures were obtained on as prepared **3** (figure 10(a)), C_3H_6 reduced **3** and C_3H_6 reduced **3** after catalysis. The surface of reduced materials and the ones after catalysis were found to be identical but very different from as prepared catalyst material **3**. Figure 10(a) gives a view of as prepared crystal of OFM **3**. The SEM pictures indicate presence of globular material in between the crystals of C_3H_6 reduced **3** rather than on the surface (figure 10(b)). A close look at the SEM pictures revealed the formation of the fibrous carbonaceous material in between the crystals of **3** (figure 10(c,d)). This amorphous material is a fibrous polymeric carbon phase bunched together and non-uniformaly distributed.

4. Conclusion

The results of this ongoing work indicate the potential application of the vanadium oxide based materials in the development of a new generation of HC-SCR deNO$_x$ catalysts. The new series of the OFM, **1**–**4**, exhibit some interesting catalytic deNO$_x$ properties. Of the four materials studied so far, **3** (the cobalt derivative) was found to be most promising for deNO$_x$ catalysis work. The catalyst derived from **3** was easily regenerated, was more tolerant towards oxygen, and remained unaffected by sample handling in air. The presence of propylene as reductant is necessary for the high deNO$_x$ activity of **3**. The active phase of the catalyst is generated during the reduction process. The very high activity associated with **3** can possibly be attributed to the cobalt centers incorporated in the vanadium oxide framework. The heterometal (cobalt) centers can play an important role in modifying the

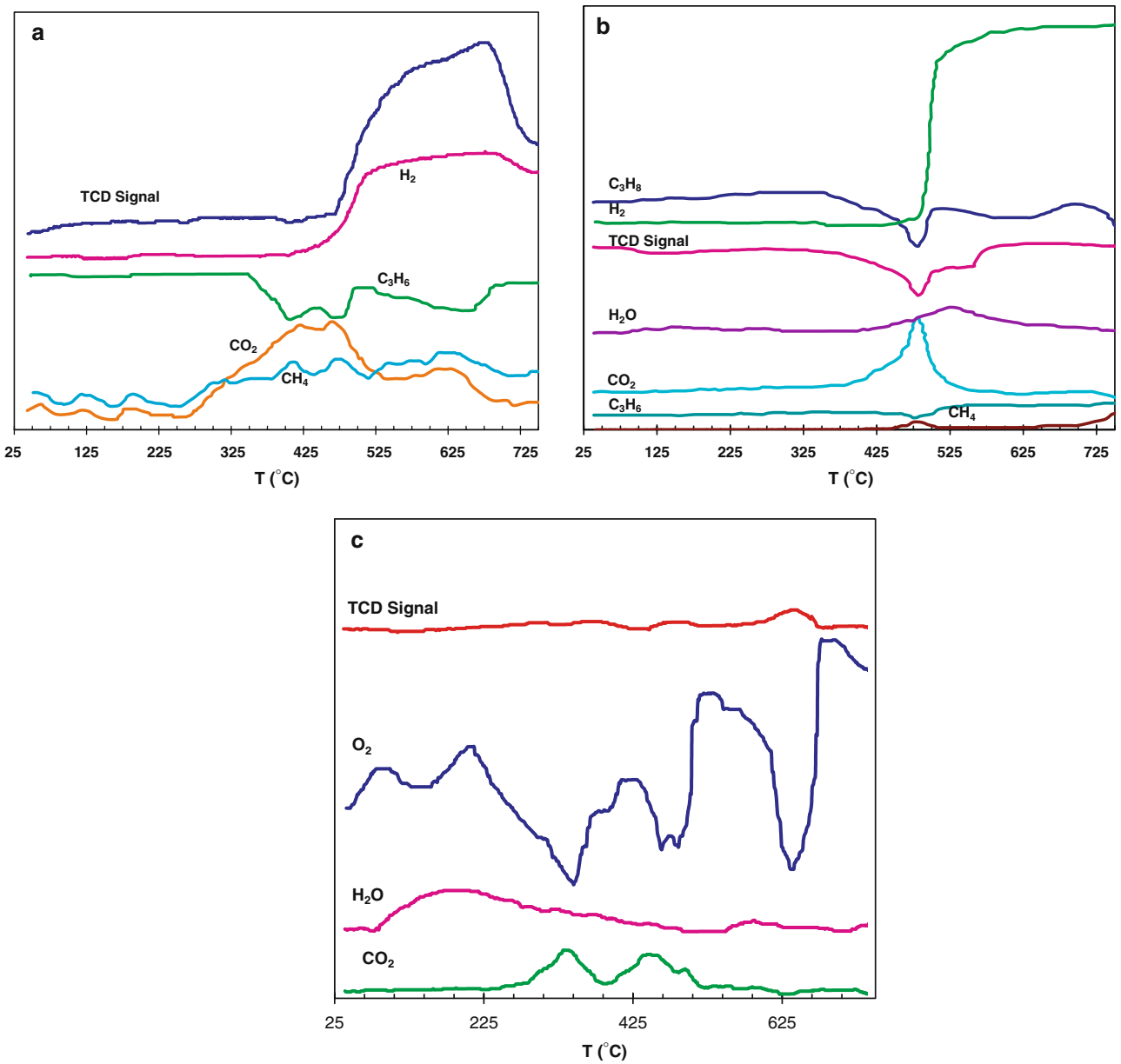

Figure 8. (a) TPR of **3** in the presence of C_3H_6. (b) Temperature programmed reduction of **3** in the presence of C_3H_8. (c) TPO of C_3H_6 reduced **3**.

electronic properties and redox chemistry of vanadium/oxo/cobalt system, making it active in the desired range for catalysis and suitable for deNO$_x$ activity. We plan to do *in situ* TPR and EXAFS studies on the catalysts to throw some light on the oxidation state and coordination sphere of working catalysts under realistic conditions (temperature, pressure, and reacting gases) and to develop a better understanding of the role of the heterometals centers and vanadium atoms in the deNO$_x$ catalysis.

The loss in crystallinity is a major problem with the long term activity of these materials. Future work will concentrate on stabilizing these catalysts towards steam deactivation. In addition, the high coking tendencies of the current catalysts imply that the use of propylene as the reductant may not be the optimal choice. Future studies will concentrate on this problem and whether these V based catalysts should be considered for HC based deNO$_x$ at all.

Finally, the work underlines the significance of the design and synthesis of new catalyst grade materials with well-defined structures containing monodispersed active sites whose properties (for example, redox property) could be fine-tuned and correlated with their structures at the molecular level. Such well-defined materials may allow fundamental studies in catalysis leading to the development of new generation of efficient catalysts.

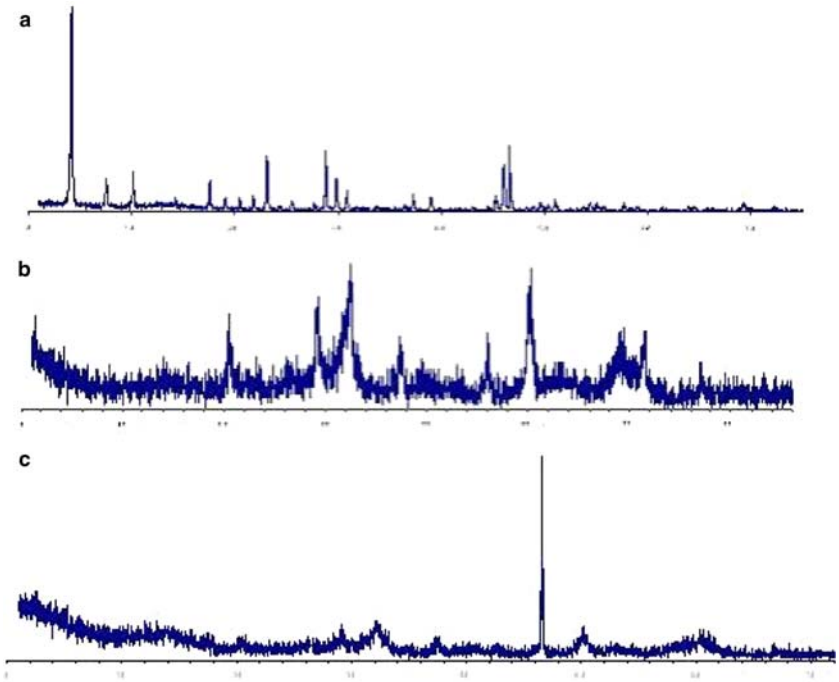

Figure 9. XRD patterns of **3** (a) As prepared. (b) After reduction in C_3H_6 at 400 °C. (c) After catalysis experiment at 500 °C.

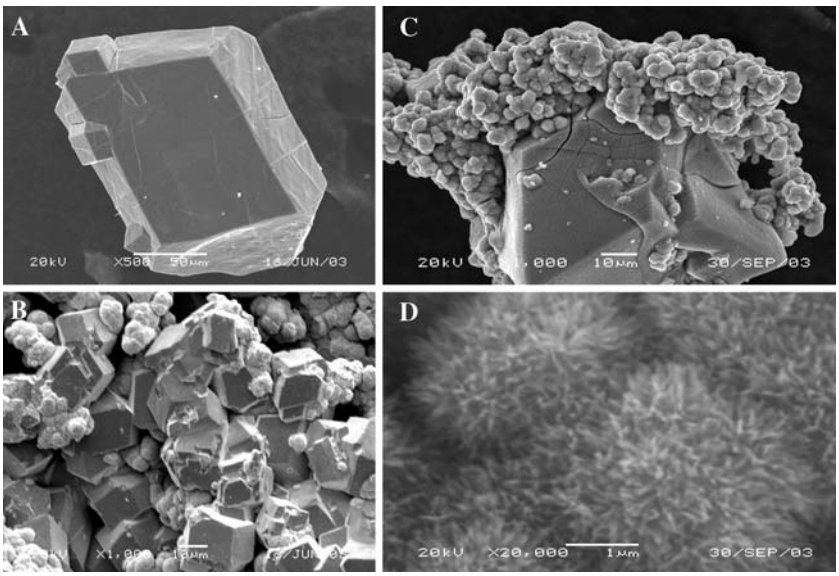

Figure 10. (a) A view of the crystal of **3** as prepared. (b) **3** after reduction with C_3H_6 indicating presence of white globular material between crystals. (c) A perspective of the white carbonaceous material present on C_3H_6 reduced **3**. (d) The carbonaceous material present between crystals of C_3H_6 reduced **3** at magnification, indicating it to be fibrous material bunched together.

Acknowledgments

This work was supported by a grant (to M.I.K.) from the NSF (CHE-0210354).

References

[1] A.D. Ellerman, *Markets for Clean Air: The U.S. Acid Rain Program* (Cambridge University Press, 2000).
[2] W.R. Moomaw, Ambio 31 (2002) 184.
[3] S. Reis, D. Simpson, R. Friedrich, J.E. Jonson, S. Unger and A. Obermeier, Atmos. Environ. 34 (2000) 4701.
[4] R.W. Howarth, E.W. Boyer, W.J. Pabich and J.N. Galloway, Ambio 31 (2002) 88.
[5] F. Nakajima and I. Hamada, Catal. Today 29 (1996) 109.
[6] M. Shelef, Chem. Rev. 95 (1995) 209.
[7] (a) L.S. Gelbov, A.G. Zakirova, V.F. Tret'yakov, T.N. Burdeinaya and G.S. Akopova, Pet. Chem. 42 (2002) 143. (b) S. Bhattacharayya and R.K. Das, Int. J. Energy Res. 23 (1999) 351.

(c) T. Kreuzer, E.S. Lox, D. Lindner and J. Leyrer, Catal. Today 29 (1996) 77.

[8] Y. Traa, B. Burger and J. Weitkamp, Micropor. Mesopor. Mater. 30 (1999) 3.

[9] (a) C.I. Round, C.D. Williams, K. Latham and C.V.A. Duke, Chem. Mater. 13 (2001) 468. (b) C.I. Round, C.D. Williams and C.V.A. Duke, Chem. Commun. 19 (1997) 1849. (c) M. Stephanopoulos, A.F. Sarofim, Y. Zhang, DOE/PC/91293, Report No. 6 (1993) (d) H. Kung, M. Kung, J.J. Spivey, B.W. Jang and F.I. Honea, DOE/PC/92521, ICCI project Number: 94-1/2.1A-2P (1995).

[10] (a) A. Corma, Chem. Rev. 97 (1997) 2373. (b) C.S. Cundy and P.A. Cox, Chem. Rev. 103 (2003) 663. (c) M.L. Occelli and H.E. Robson, *Zeolite Synthesis* (American Chemical Society, Washington, 1989). (d) P.A. Jacobs, *Zeolite Chemistry and Catalysis* (Elsevier, Amsterdam & New York, 1991). (e) J.V. Smith, Chem Rev. 88 (1988) 149.

[11] (a) M.I. Khan, E. Yohannes, R.J. Doedens, S. Tabussum, S. Cevik, L. Manno and D. Powell, Crystal Eng. 2 (1999) 171. (b) M.I. Khan, E. Yohannes and R.J. Doedens, Angew. Chem. Int. Ed. 38 (1999) 1292. (c) M.I. Khan, J. Solid State Chem. 152 (2000) 105. (d) M.I. Khan, E. Yohannes and D. Powell, Inorg. Chem. 38 (1999) 212. (e) M.I. Khan, E. Yohannes and R.J. Doedens, Inorg. Chem. 42 (2003) 3125. (f) M.I. Khan, E. Yohannes and D. Powell, Chem. Commun. 1 (1999) 23.

[12] E. Yohannes, Ph.D. Thesis, Illinois (Institute of Technology, Chicago, 2002).

[13] M.K. Neylon, M.J. Castagnola, N.B. Castagnola and C.L. Marshall, Catal Today 96 (2004) 53.